

Study on the Microstructure of Internally Oxidized Ag–Sn–In Alloys

G. Schimmel · M. Rettenmayr · B. Kempf ·
J. Fischer-Buehner

Received: 19 February 2008 / Revised: 2 June 2008 / Published online: 19 June 2008
© Springer Science+Business Media, LLC 2008

Abstract The microstructures of five internally oxidized Ag–Sn–In materials were investigated using ion polishing, field emission scanning electron microscopy and electron backscatter diffraction. The ion polished sections showed a subtle material contrast in the oxide particles that could be attributed to different oxide phases generated during internal oxidation. The phases could be identified as tetragonal SnO₂ that surrounds the cubic In₂O₃ core of the combined oxide particles. It is shown that In₂O₃ exhibits an orientation relationship to the Ag matrix and for SnO₂ and Ag another orientation relationship is likely. Interrupted internal oxidation experiments were applied to identify the growth mechanism of the oxide particles. A consistent view on the role of In during the internal oxidation of Ag–Sn–In alloys as heterogeneous nucleation agent of SnO₂ is presented.

Keywords Internal oxidation · Nucleation · Orientation relationship · Nucleation agent

J. Fischer-Buehner—Formerly with Research Institute Precious Metals & Metals Chemistry, Katharinenstr. 17, 73525 Schwaebisch Gmuend, Germany.

G. Schimmel (✉) · M. Rettenmayr
Institute of Materials Science and Technology, Friedrich-Schiller-University Jena,
Loebdergraben 32, 07743 Jena, Germany
e-mail: gunther.schimmel@uni-jena.de

B. Kempf
Umicore AG & Co. KG, Rodenbacher Chaussee 4, 63457 Hanau-Wolfgang, Germany

Present Address:
J. Fischer-Buehner
Legor Group Srl, Vicenza, Italy

J. Fischer-Buehner
Indutherm GmbH, Walzbachtal, Germany

Introduction

For many industrial applications it is necessary to reinforce the strength of noble metals like Ag and Pt. One of the options for strengthening is dispersion hardening with oxide particles, generated, e.g. by internal oxidation. Internal oxidation results from oxygen diffusion into the alloy and the formation of stable oxide particles with the less noble alloying components inside the grains. Ag-based materials are widely used for electrical contacts in the automotive industries. Formerly Ag contacts were strengthened with CdO. Due to the ban of Cd in electrical applications an alternative for the Ag–CdO had to be found. Consequently, extensive research has been conducted on Ag–SnO₂–In₂O₃ contact materials produced by internal oxidation as an alternative [1, 2]. For adjusting the switching behavior of the electrical contacts for specific applications, it is essential to control morphology and dispersion of the oxide particles. Understanding the growth mechanism of the oxide particles in Ag–Sn–In alloys during internal oxidation is thus a prerequisite for optimized materials properties. Experimental investigations on nucleation, allocation and orientation relationships of the oxide phases during the internal oxidation are the central aspects of the present work. Some information on oxide particle morphology and crystallography of oxidized Ag–Sn–In alloys is documented in the literature. Douglass [3] discusses that the shape of the oxide particles can vary in a wide range, depending on oxidation conditions and alloy composition. The dependence of the oxide particle morphology in Ag–Sn–In alloys on the oxygen partial pressure and oxidation temperature is investigated in [4, 5]. Qualitatively it can be stated that lowering oxidation temperatures and raising oxygen partial pressures results in a refinement of the oxide particles. The influence of the annealing time on the morphology of the oxide particles is only relevant for nano-scale oxide particles which are exposed to temperatures next to the melting point of Ag [6]. Osada et al. [7] have shown that the oxide particle morphology of internally oxidized Ag–Sn–In alloys strongly depends on the fraction x_{Sn} of the alloy. This fraction describes the ratio of Sn atoms to the sum of Sn and In atoms in the alloy (Eq. 1). It was found that Sn-rich Ag–Sn–In alloys form globular oxide particles, whereas in In-rich Ag alloys a needle-like or fishbone-like shape of the oxide particles is prevalent [2, 7].

$$x_{\text{Sn}} = \frac{c_{\text{Sn}} [\text{at.}\%]}{c_{\text{Sn}}[\text{at.}\%] + c_{\text{In}}[\text{at.}\%]} \quad (1)$$

In the absence of In, Ag–Sn alloys have a strong tendency to form oxide bands [8–10] similar to the periodic oxide bands observed in internally oxidized Ag–Mg alloys [11, 12]. Ternary In additions of more than 2 wt.% accelerate the internal oxidation kinetics and avoid internal oxide bands [1] in Ag–Sn alloys. Osada et al. [7] could show by using X-ray diffraction (XRD) for oxidized Ag–Sn–In alloys that the existence of tetragonal SnO₂ and body-centered cubic In₂O₃ crystals in the Ag matrix is strongly dependent on the x_{Sn} fractions in the precursor alloy. For low x_{Sn} fractions no diffracted X-rays from the SnO₂ crystals were observed by means of XRD [7]. It was found that in a material containing low Sn concentrations most of the Sn atoms are dissolved in the In₂O₃-lattice during oxidation [7]. With standard mechanical metallographic preparation methods and scanning electron microscope

techniques (e.g. mappings by means of Energy Dispersive X-ray analysis (EDX)) it is not possible to determine quantitatively the spatial distribution of the In_2O_3 and SnO_2 in the microstructure of the oxidized alloy. Due to similar excitation energies of Ag, Sn and In the L- and K-excitations overlap in the EDX-spectrum and prevent a quantification of the elements. As a result the exact spatial allocation of In_2O_3 and SnO_2 in the oxidized alloy has not been so far described in the literature. It is also unknown whether In_2O_3 and SnO_2 are combined in common oxide particles or form separate ones. The existence of an orientation relationship between the oxide particles and the surrounding Ag has not been investigated in detail yet. On the basis of differences in the standard enthalpy of formation, Verma and Anantharaman [4] assume that In_2O_3 might be a nucleation agent for SnO_2 precipitation. Clarifying those issues is crucial for understanding the role of In during the nucleation of SnO_2 in Ag–Sn–In alloys.

The aim of the present paper is not to determine the oxide morphology depending on a change of several oxidation conditions as already published in [4, 5, 7]. It is aspired to identify the spatial distribution of In_2O_3 and SnO_2 in Ag– SnO_2 – In_2O_3 materials as well as the orientation relationships between the oxide particles and Ag. The study is carried out by means of new analyzing and preparation techniques like electron back scatter diffraction (EBSD) and ion polishing. The influence of In in the alloy for the nucleation and oxide particle growth on the internal oxidation front of an interrupted internal oxidation is also clarified.

Experimental Procedure

For the investigations five internally oxidized Ag–Sn–In alloys were used. Composition of the alloys and oxidation temperatures are listed in Table 1. In Table 1 also the x_{Sn} fraction (Eq. 1) is listed. The specimens were melted in a graphite crucible under high purity Ar atmosphere. As starting materials for melting pure Ag (99.9999%), In and Sn (99.99%) were used. The cast ingots (36 mm in diameter) were homogenized in Ar atmosphere for 20 h at 1,023 K. Afterwards the cylindrical ingots were extruded and drawn to wires. Standard metallographic preparation including etching with $\text{NH}_3\text{--H}_2\text{O}_2$ and optical microscopy was used to verify the absence of second phases in the Ag solid solution.

The alloy wires were oxidized in a furnace with streaming oxygen (materials A, B, C, D) and in a pressure furnace (material E). All samples except material D

Table 1 List of alloys and oxidation condition (concentrations in weight-percent)

Material	A	B	C	D	E
Ag [wt.%]	95.9%	92.6%	89.0%	89.0%	87.6%
Sn [wt.%]	1.2%	4.4%	6.9%	6.9%	8.1%
In [wt.%]	2.9%	2.9%	4.2%	4.2%	4.3%
x_{Sn} fraction	0.28	0.59	0.62	0.62	0.65
Temperature [K]	1023	1023	1023	873	873

(240 h) were oxidized in 38 h. Afterwards sections perpendicular to the wire axis were prepared by standard metallographic preparation. The deformation zone of the last mechanic polishing step was removed by ion polishing. For the scanning electron imaging a scanning electron microscope with field emission gun (SEM-FEG) was used. Considering the dependence of the average particle radius and spacing on their distance to the sample surface in internally oxidized alloys [13] all observations were accomplished at approximately the same distance below the wire surface ($\sim 400 \mu\text{m}$). Also a thin foil was prepared by focused ion beam (FIB) out of a section of material C and thinned to a lamella with gallium ions for investigations in the transmission electron microscope (TEM). For further TEM investigations a specimen out of material D was prepared by mechanical polishing and wet chemical etching with $\text{NH}_3\text{-H}_2\text{O}_2$.

Results

Characterization of the Oxide Particles

The ion polishing allowed the identification of subtle material contrasts in the oxide particles by using the backscattered and “through lens” detectors on the SEM-FEG. It was detected, that in materials B, C, D and E different phases can be distinguished in the oxide particles (Figs. 1–4). The two oxide phases are labeled below and in the following figures (Figs. 1–5) as phase I and II. Additional topography contrasts marked with circles in Figs. 1 and 3 are caused by slopes and dents of the ion polished surface and considered as independent from the material contrasts. The parallel lines and different shades of grey in the Ag matrix are twins (e.g. see Fig. 3). These crystallographic features are visible due to the horizontal orientation contrast of the back-scattered electrons [14] on the ion polished surfaces.

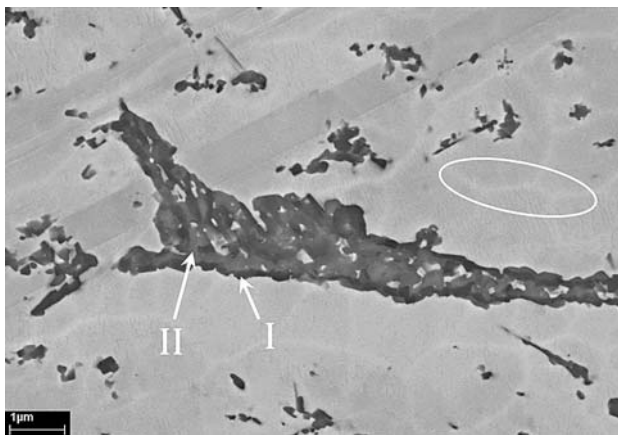


Fig. 1 Microstructure of material B; backscattered electrons were used for imaging the material contrast in oxide particles on an ion polished section; additional topography contrast (slopes and dells) is visible in the Ag matrix caused by the ion polishing

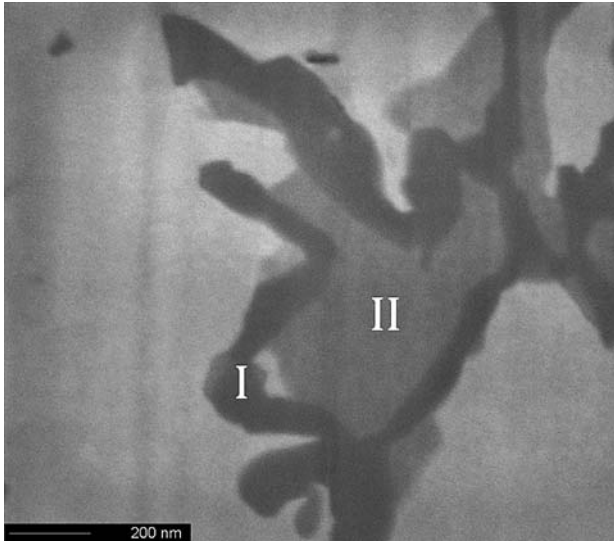


Fig. 2 Microstructure of material C; “through lens” secondary electron image of an ion polished section features similar material contrasts as materials B, D and E

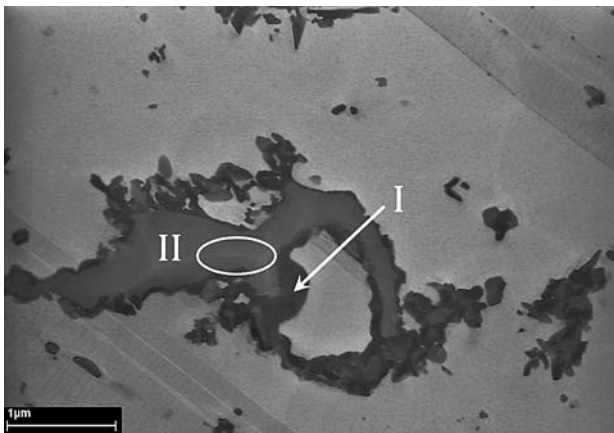


Fig. 3 Microstructure of material D; “through lens” secondary electron image of an ion polished section features similar material contrasts as materials B, C and E; horizontal lines in the Ag matrix are twin borders

It was also checked whether the oxidation temperature or the amounts of alloying elements in the precursor alloy have an influence on the appearance of the material contrast in the oxide particles. Materials C and D (Figs. 2 and 3) show that the oxidation temperature has no significant influence on the appearance of the material contrast. Even the variation of the total amount of alloying elements between materials B and C do not change the phase appearance (Figs. 1 and 2), the darker

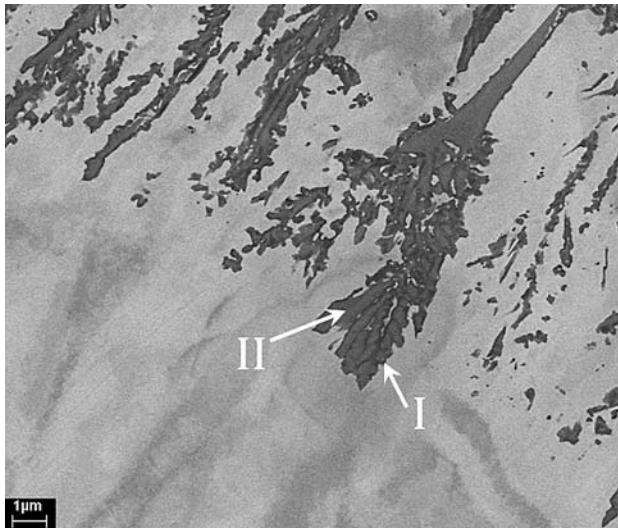


Fig. 4 Microstructure of material E; backscattered electrons were used for imaging the material contrast on an ion polished section; the internal oxidation was interrupted to investigate the In_2O_3 and SnO_2 growth on the internal oxidation front

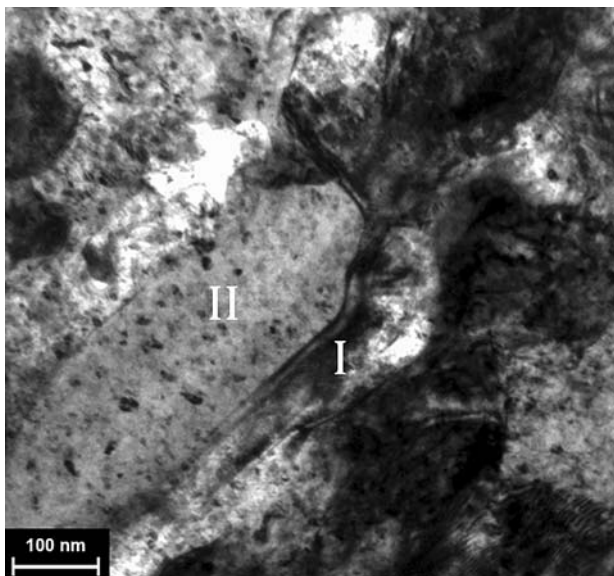


Fig. 5 TEM-image of an $\text{In}_2\text{O}_3/\text{SnO}_2$ particle in the FIB prepared TEM foil of material C; contrasts in the particle were superimposed by strain fields of the Ag matrix below and above the oxide particle

Sn-rich phase still covers the brighter In-rich phase in numerous oxide particles. Material A (Fig. 6) illustrates that changes in fraction x_{Sn} (Eq. 1) of the precursor alloy can cause the disappearance of the material contrast. It is a fact [7] that for

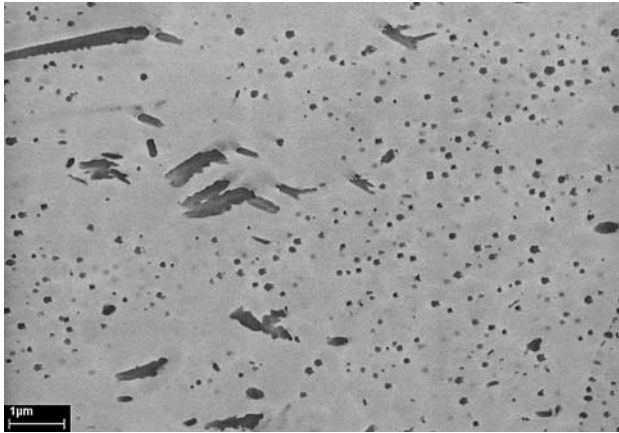


Fig. 6 Microstructure of material A; “through lens” secondary electrons were used on an ion polished section; material contrasts in the oxide particles are not visible

intermediate fractions x_{Sn} the oxide particles feature a fishbone-like morphology and grow approximately in the direction of the moving internal oxidation front. It was observed that the internal oxidation front is not a straight line when fishbone-like oxide particles are present. It is expanding to a reaction zone in which the large elongated oxide particles are growing ahead of the smaller particles as shown in Figs. 4, 9a and 10a. The tip of the growing elongated oxide particles consisted of phase II, which was not covered with phase I (zones of interest are marked with white ellipsoids in Fig. 9a). Besides the combined In_2O_3/SnO_2 particles, e.g. the microstructure of material D features also oxide particles without In_2O_3 inside the particles due to the intermediate x_{Sn} fraction of the material. TEM imaging of those particles revealed a distinct inner structure (Fig. 7). This kind of oxide particles

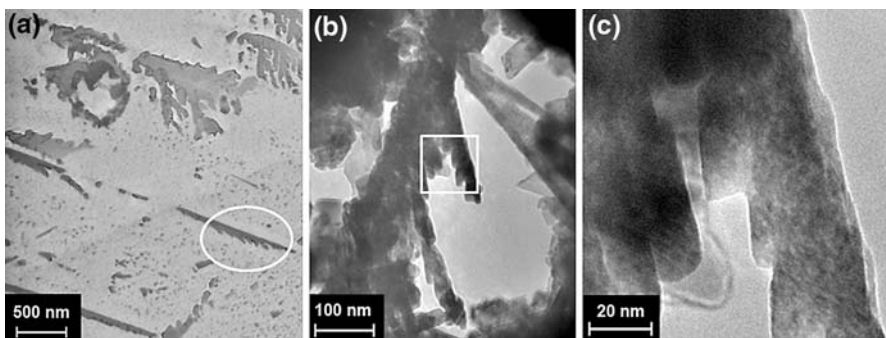


Fig. 7 An orientated plate-like inner structure in elongated oxide particles containing SnO_2 without the In_2O_3 phase in the particle center in material D; a similar oxide particle as the marked particle in SEM-FEG micrograph (a) is shown in TEM images (b) and (c)

seems to consist of a series of orientated plate-like SnO_2 crystals arranged stackwise in the direction of longest dimension of the oxide particle (Fig. 7).

Allocation of Material Contrasts

For characterizing the composition of phases I and II, EDX spectra of the two phases were established. As already mentioned quantitative analyses and EDX mappings are not possible due to the overlap of the L-series peaks of Ag, In and Sn and the width of the energy windows for quantification. For example the $\text{In-L}\beta_1$ peak is situated in the same energy window like the $\text{Sn-L}\alpha_1$ peak. Working with low acceleration voltages on the SEM-FEG the excited volume can be situated within an oxide particle and Ag's L-series peaks do not interfere the In and Sn excitations (Fig. 8). Then it is possible to obtain qualitative information of the presence of these elements by tracing the $\text{L}\alpha_1$ -peaks of In and Sn in the spectrum. Prerequisite is that the $\text{L}\alpha_1$ peak of Sn can prevail as compared to the overlapping $\text{L}\beta_1$ peak of In. This case is shown in EDX spectrum (Fig. 8a) of phase I obtained from the oxide particle in Fig. 3. The excitation spectrum shows that phase I is Sn-rich with only very weak In-signal. The spectrum of phase II on the other side features overlapping peaks of the L-series of Sn and In (Fig. 8b) that means both elements are found in phase II. Considering the excited volume in the EDX analysis in the bulk material, the EDX measurements were repeated on similar shaped oxide particles in the FIB-prepared TEM-foil (Fig. 5). By means of the higher lateral resolution of TEM-EDX the results of the EDX measurements in the bulk material were confirmed. To determine the crystal structure of phase I and II a crystallographic study was carried out with ion polished sections of material E by means of EBSD. Phase I was identified as a tetragonal SnO_2 crystal lattice (Figs. 9 and 10c). Phase II was identified as cubic and therefore could not be distinguished clearly from the face-centered-cubic (fcc) Ag

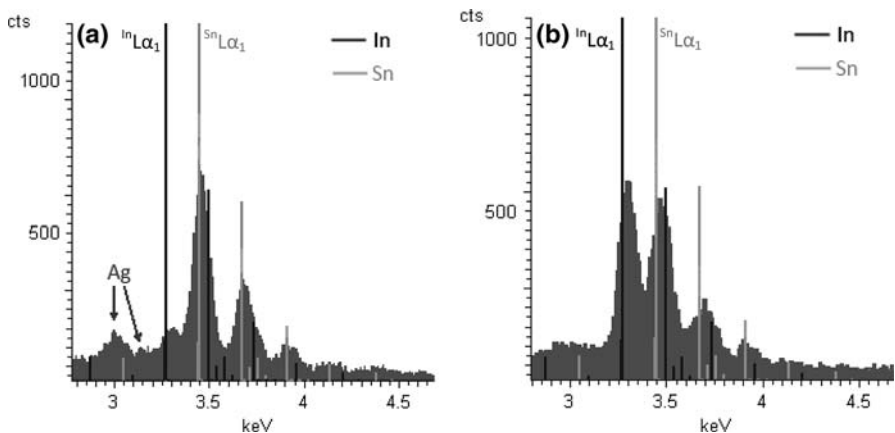


Fig. 8 EDX-spectra of phase I (a) and II (b) as taken from the oxide particle shown in Fig. 3; the overlapping L-Series of In and Sn are labeled in the excitation spectra

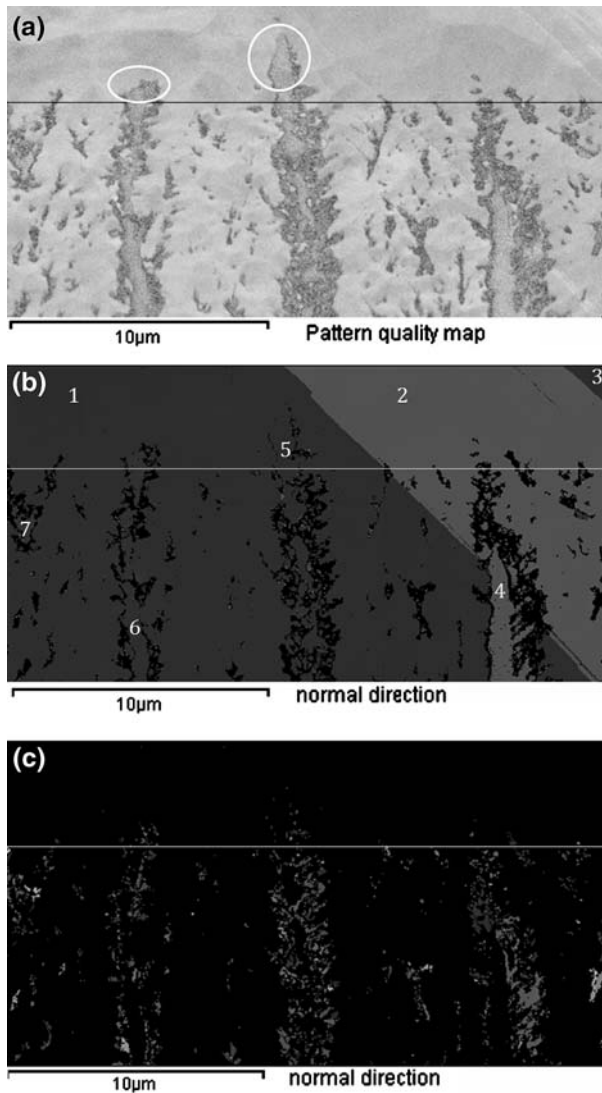
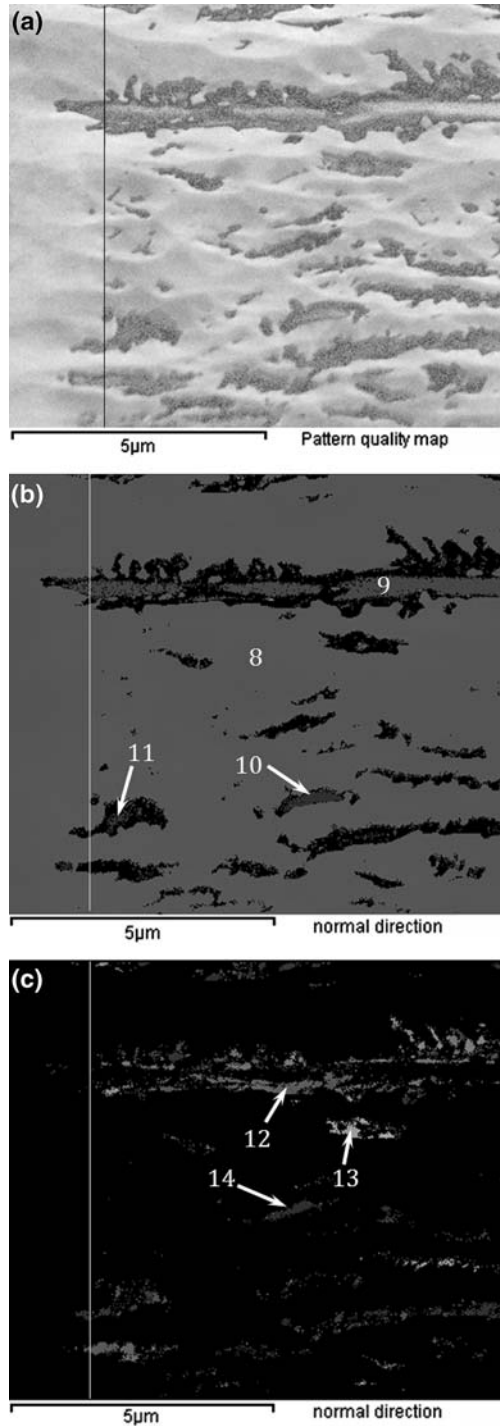


Fig. 9 EBSD mapping of an area along the internal oxidation front of material E; orientation maps feature individual crystal orientation with respect to the sample normal; (a) acquired quality of the Kikuchi pattern, (b) orientation of the cubic crystals (Ag and In₂O₃), (c) orientation of the tetragonal SnO₂ phase

lattice in terms of phase separation by the EBSD-system (Figs. 9b and 10b). Considering the EDX spectrum of phase II in the oxide particles (see Fig. 8b) phase II is considered to be a body-centered-cubic (bcc) In₂O₃ lattice in agreement with the material contrast of the SEM-FEG images. The Sn signals in the spectrum of Fig. 8b could be attributed to solute Sn atoms in the In₂O₃ lattice as described in [7] and the adjacent tetragonal SnO₂-phase.

Fig. 10 EBSD mapping of an area along the internal oxidation front of material E; orientation maps feature individual crystal orientation with respect to the sample normal; (a) acquired quality of the Kikuchi pattern, (b) orientation of the cubic crystals (Ag and In_2O_3), (c) orientation of the tetragonal SnO_2 phase



Orientation of the Oxide Phases

In addition to the phase identification it is possible to image differences in crystal orientation between the fcc Ag and the bcc In_2O_3 phase by means of EBSD. The individual crystal directions are displayed with respect to the specimen's axis (e.g. to the specimen normal which is parallel to the wire axis). The orientation analysis of the EBSD measurements yields that the Ag crystals have distinct lattice planes orientated along the wire axis. In all of the Ag crystals the normal to either the $\{111\}$ - or the $\{001\}$ -planes was parallel to the wire axis. This feature is well known as a fibre texture in fcc materials and can be attributed to the extrusion of the wires before oxidation. Due to the low stacking fault energy the Ag crystals exhibit several twins which can be observed as a rotation around the normal axis of one of its close-packed $\{111\}$ -planes. The Ag crystals No. 1 and No. 2 in Table 2 and Fig. 9 are an example of this twin orientation relationship. Concerning orientation relationships of the oxides, it was detected that the orientation of the In_2O_3 particles is correlated with the orientation of the surrounding Ag crystal. If the Ag is orientated with, e.g. one of its $\langle 111 \rangle$ directions parallel to the wire axis the In_2O_3 can grow in the same orientation as the surrounding lattice or it can be tilted, so that one of the $\langle 001 \rangle$ directions is parallel to the wire axis (Fig. 9 and Table 2). For $\langle 001 \rangle$ Ag directions parallel to the wire axis the orientations of In_2O_3 particles are $\langle 111 \rangle$ (Fig. 10 and Table 2). For the case that both phases have the same orientation with respect to the wire axis the crystal orientation vertical to wire axis can be identical (No. 1 and No. 5 in Table 2) or rotated around the $\langle 111 \rangle$ direction of both crystals which is parallel to the wire axis. The angle of the rotation is approximately 60° . This behavior can be observed on crystals No. 1 and No. 7 in Table 2 and Fig. 9b, which have their $\langle 111 \rangle$ directions orientated parallel to the wire axis. Obtaining the orientation information of the SnO_2 phase with respect to Ag and

Table 2 Crystal orientation and type of phase corresponding to numbers 1–14 in Figs. 7 and 8

No. in EBSD-maps	Phase	Crystal structure	Crystallographic axis parallel to wire axis
1	Ag	fcc	$\langle 111 \rangle$
2	Ag	fcc	$\langle 001 \rangle^a$
3	Ag	fcc	$\langle 111 \rangle$
4	In_2O_3	bcc	$\langle 001 \rangle$
5	In_2O_3	bcc	$\langle 111 \rangle$
6	In_2O_3	bcc	$\langle 111 \rangle$
7	In_2O_3	bcc	$\langle 111 \rangle^b$
8	Ag	fcc	$\langle 001 \rangle$
9	In_2O_3	bcc	$\approx \langle 001 \rangle$
10	In_2O_3	bcc	$\langle 111 \rangle$
11	In_2O_3	bcc	$\langle 111 \rangle$
12	SnO_2	Tetragonal	$\approx \langle 001 \rangle$
13	SnO_2	Tetragonal	$\langle 001 \rangle$
14	SnO_2	Tetragonal	$\langle 110 \rangle$

^a Compared to the orientation of the Ag crystal No. 1 it exhibits a rotation around a $\langle 111 \rangle$ axis

^b Compared to the orientation of the surrounding Ag lattice (No. 1) the crystal exhibits a rotation around the $\langle 111 \rangle$ axis which is parallel to the wire axis

In_2O_3 is tedious because the SnO_2 phase features a poor image quality of the Kikuchi pattern in the EBSD analysis (Figs. 9a and 10a). Only a few areas on the sample provided a suitable image quality to determine the orientation of the SnO_2 phase as showed in Fig. 10c (Nos. 12–14 in Table 2).

Discussion

Interrelation of In_2O_3 and SnO_2

In the present study two central aspects of the role of In_2O_3 during internal oxidation of Ag–Sn–In alloys were detected. For the first time it was possible to identify a material contrast within the oxide particles of oxidized Ag–Sn–In alloys. The material contrast in the oxide particles could be assigned to two oxide phases (In_2O_3 and SnO_2) by means of EBSD supported by qualitative EDX information. Considering the material contrast in the SEM-FEG results, it can be stated that almost all In_2O_3 particles were covered with SnO_2 . Variations of the oxidation temperature in the range of 873–1,073 K and changes in the total amount of alloying elements in the precursor alloy had an effect on the mean particle radius and spacing as already known from [4, 5]. The focus of this study was on the fact that they do not have a distinctive effect on the appearance of the combined $\text{In}_2\text{O}_3/\text{SnO}_2$ particles. Solely the x_{Sn} fraction was found to have an influence on the appearance of the material contrast within the oxide particles. Osada et al. showed by means of XRD measurements that the lattice parameter of In_2O_3 -crystals increases with increasing Sn content in the oxidized alloy [7]. In addition Osada's investigation revealed that in oxidized alloys with low x_{Sn} fractions no diffracted beams of the (101)-planes of the tetragonal SnO_2 lattice were found. The formation of a substitution mixed crystal containing In_2O_3 and Sn proposed by Osada et al. [7] is also favored as explanation for the missing material contrasts in material A (low x_{Sn} fraction) in our study.

Orientation Relationship Oxide Particles—Matrix

The second aspect of this study was to clarify possible orientation relationships between SnO_2 or In_2O_3 and the Ag matrix. For summarizing the orientation relationships between Ag and In_2O_3 crystals the tilt of the oxide crystal lattice against the wire axis and its rotation around the wire axis have to be considered in the fibre-textured Ag matrix. Three types of orientation relationships between Ag matrix and In_2O_3 particles were found:

- (1) In_2O_3 and Ag can be orientated uniformly, that means no rotation around or tilt against the wire axis occurs.
- (2) In_2O_3 and Ag crystals are not tilted against each other, but In_2O_3 is rotated approximately 60° around an (111)-pole which is parallel to the wire axis. This orientation relationship can be described as a twin relationship of cubic crystals.

- (3) In_2O_3 is tilted approximately 54° against the wire axis compared to the Ag matrix. In this case the crystallographic direction parallel to the wire axis for In_2O_3 is $\langle 111 \rangle$ or $\langle 100 \rangle$ and for Ag $\langle 100 \rangle$ or $\langle 111 \rangle$, respectively.

An orientation relationship of SnO_2 and In_2O_3 and also SnO_2 and Ag is possible. The TEM images indicate that there is an orientated growth of SnO_2 crystals in Ag, too. However to prove an orientation relationship concerning SnO_2 high resolution transmission electron microscopy techniques would be more adequate than EBSD. EBSD suffers in this case from the low quality of the Kikuchi pattern of SnO_2 . This is an indication that SnO_2 crystals contain more lattice defects than the In_2O_3 or the surrounding Ag. Further investigations have to be carried out to clarify this matter.

Aspects of Nucleation and Growth of Oxide Particles

In former studies concerning the role of In inside of oxidizing Ag–Sn–In alloys [4] it was suggested that In_2O_3 facilitates the nucleation of SnO_2 . This theory is motivated by the slightly higher thermodynamic stability of the In_2O_3 compared with SnO_2 . This approach does not include aspects like nucleation, lattice strains and crystallographic orientation relationships. However in the present study it is shown that In_2O_3 is located in the core of the combined $\text{SnO}_2/\text{In}_2\text{O}_3$ particles and it was observed that In_2O_3 precipitates ahead of SnO_2 using interrupted internal oxidation experiments. This behavior can be attributed to the higher free energy of formation of In_2O_3 but also to the orientation relationship between In_2O_3 and Ag which facilitates the nucleation of the In_2O_3 particle due to the reduction of the interfacial energies and the elastic lattice strains. Once In_2O_3 has nucleated a growth selection of the nuclei will occur. In_2O_3 nuclei which have their fastest growing crystallographic direction approximately parallel to the moving direction of the internal oxidation front will grow faster and govern the growth conditions in their neighborhood. The growth of the In_2O_3 results in a local loss of solute In atoms in the fcc Ag matrix which increases the relative Sn content of the matrix. In [7] it is shown that the In_2O_3 lattice dissolves Sn atoms which decreases the local Sn content. This effect can partly compensate the relative increase of Sn atoms in the neighborhood of the growing In_2O_3 particles. However it is supposed that at the latest when In_2O_3 lattice is saturated with Sn atoms, tetragonal SnO_2 crystallizes on the In_2O_3 –Ag interface and coats the In_2O_3 particle. For this last aspect it is possible that an orientation relationship between both SnO_2 and In_2O_3 exists, even though this has not been shown conclusively yet. The reason for the growth of the elongated oxide particles ahead of the main internal oxidation front is the advantage of time compared with other oxide particles which undergo an incubation period before nucleating.

Conclusion

In this study for the first time it was possible to observe material contrasts of SnO_2 and In_2O_3 within the oxide particles of Ag– SnO_2 – In_2O_3 materials. In_2O_3 forms the

core of numerous oxide particles and grows ahead of the smaller oxide particles at the internal oxidation front in the shape of elongated oxide particles. These In_2O_3 crystals are covered with a layer of SnO_2 during the oxidation process. Thus it is shown that In_2O_3 acts as a heterogeneous nucleation agent for SnO_2 in Ag. As a result Ag– SnO_2 – In_2O_3 contact materials produced by internal oxidation feature combined oxide particles consisting of In_2O_3 and SnO_2 in contrast to separate oxide particles which are found in Ag– SnO_2 – In_2O_3 produced by other manufacturing processes like powder metallurgy. Three orientation relationships between In_2O_3 and Ag were detected by means of EBSD and hints for further orientation relationships between SnO_2 /Ag and SnO_2 / In_2O_3 were observed. It is assumed that the orientation relationship between Ag and In_2O_3 facilitates the nucleation of In_2O_3 during internal oxidation.

Acknowledgement The authors are thankful to the workgroup of Prof. Muecklich of the Saarland University for using their FIB preparation facilities. Thanks also to Mr. Ommer and Mrs. Bretzler of the *Research Institute Precious Metals & Metals Chemistry*, Schwaebisch Gmuend for their technical assistance.

References

1. A. Verma, A. Roy, and T. R. Anantharaman, *The International Journal of Powder Metallurgy* **27**(1), 51 (1991).
2. A. Verma and T. R. Anantharaman, *Journal of Material Science* **27**, 5623 (1992).
3. D. L. Douglass, *Oxidation of Metals* **44**(1/2), 81 (1995).
4. A. Verma and T. R. Anantharaman, *Bulletin of Material Science* **14**(1), 1 (1991).
5. W. Kunert and P. Leis, *Zeitschrift Metall.* **47**(1), 18 (1993).
6. K. Sakairi, H. Tsuji, and K. Tsuchiya, in *28th Holm Conference on Electrical Contacts* (1982).
7. M. Osada, Y. Amano, T. Igarashi, S. Ikeda, A. Fukui, and S. Ochi, in *International Conference on Electrical Contacts (ICEC)* (Berlin, 1982).
8. M. Bruncko, I. Anzel, and A. C. Kneissl, *Corrosion Science* **49**, 1228 (2007).
9. J. W. Lee and H. C. Lee, *Scripta Materialia* **42**, 169 (2000).
10. M. Bruncko, A. C. Kneissl, and I. Anzel, *Praktische Metallographie* **44**(10), 464 (2007).
11. D. L. Douglass, B. Zhu, and F. Gesmundo, *Oxidation of Metals* **38**(5/6), 365 (1992).
12. L. Charrin, A. Becquart-Gallissian, A. Combe, G. Gonzalez, and A. Charai, *Oxidation of Metals* **57**(1/2), 81 (2002).
13. M. Kahlweit, *Zeitschrift fuer Physikalische Chemie (Muenchen, Germany)* **32**, 1 (1962).
14. A. P. Day and T. E. Quested, *Journal of Microscopy-Oxford* **195**, 186 (1999).